Crystallization, Melting, and Morphology of Low Molecular Weight Polyethylene Fractions

Gary M. Stack and Leo Mandelkern*

Department of Chemistry and Institute of Molecular Biophysics, Florida State University, Tallahassee, Florida 32306

Ingrid G. Voigt-Martin

Institut für Physikalische Chemie, Johannes-Gutenberg-Universität, D-65 Mainz, West Germany. *Received May 3, 1983*

ABSTRACT: The crystallization, melting, and morphology of low molecular weight fractions of linear polyethylene, $M_n = 1.6 \times 10^3$ to 8.0×10^3, have been studied in detail. In this molecular weight range it is possible under appropriate crystallization conditions, to form extended-chain crystals as well as much smaller size crystallites. When this size change occurs in the same molecular weight fraction, it does so rather abruptly with only a small change in the crystallization temperature. Detailed studies of the course of the isothermal crystallization, utilizing the low-frequency Raman acoustical mode as a major diagnostic tool, along with thermodynamic measurements, have led to an understanding of the crystallization process and of the size differences. The melting temperatures of the extended-chain crystals have been analyzed according to Flory's theory. The problems involved in extrapolating to infinite molecular weight have been put into proper perspective. Transmission electron micrographs for a fraction $M_n = 5600$ crystallized at different temperatures have also been studied. Roof-shaped lamellae, with a lateral extension of several microns, are observed even for quenched samples. Analysis of the apex angles determines the angle of inclination between the chain axis and the lamellar normal. This tilt angle is found to be dependent on the crystallization conditions.

Introduction

The crystallization and melting behavior of low molecular weight fractions of several polymers, particularly poly(ethylene oxide), have been studied in detail.[1-7] The crystallization of such samples is of fundamental importance because of the relative crystallite thicknesses that can be developed. In this molecular weight range under appropriate crystallization conditions it is possible to form crystallites whose thicknesses are comparable to the extended-chain length of the molecule. It is, of course, also possible to develop much smaller sizes in the same sample. The melting of such samples is of interest since it should be possible, by proper analysis, to obtain information with respect to the interfacial free energies as well as the equilibrium melting temperatures. There is some confusion in the literature on how to properly analyze such data.[1,8] Some basic theoretical problems exist that need to be examined in detail. The poly(ethylene oxide) studies in this molecular weight range have resulted in many unusual results.[2-4] One very striking observation has been that it is possible for a significant increase in crystallite thickness and melting temperature to result with only a small change in the crystallization temperature.

There has been, heretofore, very little detailed study of the low molecular weight polyethylenes. One reason may be that narrow fractions in the low molecular weight range have not been easily available. There are several reasons why a study of the crystallization behavior of the polyethylenes would be advantageous. The question as to the general nature of the poly(ethylene oxide) results as well as their interpretation could be answered. The polyethylene end groups are relatively noninteractive as compared to the usual hydroxyl end groups of poly(ethylene oxide), where specific interactions are likely. Moreover, there is a set of standard well-accepted thermodynamic data for the *n*-hydrocarbons[9,10] which can serve as a reference and basis of comparison for data obtained for the extended-chain crystals. Recent developments in Raman spectroscopy, utilizing the low-frequency longitudinal acoustic mode, have allowed for the determination of the crystallite size distribution in polyethylene and, presumably, in other polymers as well.[11-13,47] Thus, it is now possible to study the fusion of such samples knowing the intial crystallite size distribution as well as any changes that take place with thermal treatment. We have, therefore, assembled a set of narrow molecular weight distribution linear polyethylene samples and have studied their crystallization behavior in detail. The unique character of these samples, along with developments in electron microscope techniques,[14-17] has made it advantageous to also examine selected samples by this technique.

Table I
Molecular Weights of Polyethylene Fractions

M_n	M_w	M_w/M_n
1586	1756	1.11
2221	2496	1.12
3769	4116	1.09
5600	5800	1.04
8000	8400	1.05

Experimental Section

The molecular weight characteristics of the fractions used in this work are given in Table I. The three lowest molecular weight samples were obtained by a fractionation procedure previously described.[18] Two of the fractions, $M_n = 1586$ and $M_n = 3769$, were actually used in earlier work.[19] The two highest molecular weight samples were obtained from Societé National Elf Aquitaine (SNEA). The molecular weights of all the fractions were obtained by gel permeation chromatography.

The low-frequency Raman longitudinal acoustical modes were obtained with a Spex 1403 double-monochromator Raman spectrometer, the details of which have been described previously.[13,20] The observed spectra were analyzed according to the procedures given by Snyder and Scherer,[11,12] to yield a distribution of crystallite thicknesses.

The specimens were also examined by thin-section electron microscopy. The relatively mild preparative techniques that have been previously described in detail were again used.[15-17]

The melting behavior was studied with a Perkin-Elmer DSC 2B differential calorimeter. In a standard experiment about 1.0 mg of sample was used, and the heating rate was 5 °C/min. The peak in the endotherm was taken as the melting temperature.

In general, for polymers the location of this peak will depend on heating rate and sample mass.[21,22] Furthermore, we have recently shown that even after extrapolation to low heating rates and sample mass the position of this peak cannot be used as an

0024-9297/84/2217-0321$01.50/0

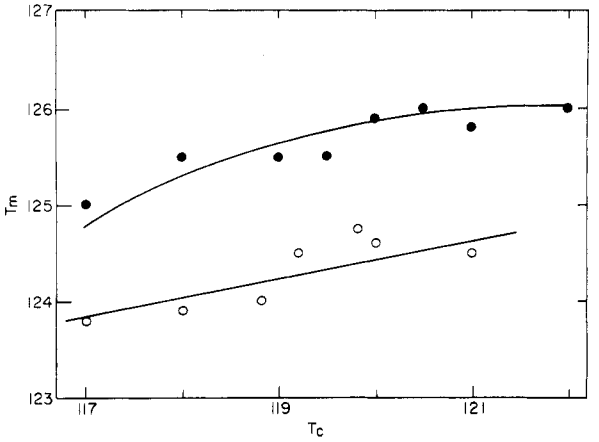

Figure 1. Plot of observed melting temperature, T_m, against crystallization temperature, T_c: (○) for fraction M_w = 1756, M_n = 1586; (●) for fraction M_w = 2496, M_n = 2221.

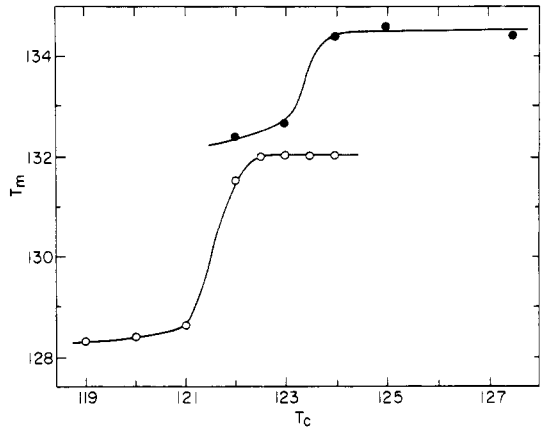

Figure 2. Plot of observed melting temperature, T_m, against crystallization temperature, T_c: (○) for fraction M_w = 4116, M_n = 3769; (●) for fraction M_w = 5800, M_n = 5600.

absolute or even a relative melting temperature.[23] However, it was also shown in the work cited[23] that in the low molecular weight range of interest here these problems do not exist. It was found that the endothermic peak was insensitive to the above parameters and gave a very good measure of the true melting temperature. Hence in this work we have taken the melting temperature determined in the manner described above as representing the true one and used it in the required theoretical calculations.

Results and Discussion

Crystallization and Melting. Each of the molecular weight fractions was isothermally crystallized over the accessible temperature range in order to study the dependence of the melting temperature on the crystallization temperature. Measurements were made on samples that were held at the crystallization temperature for sufficiently long times to ensure the essential completion of the process. The highest observed melting temperature for each crystallization temperature was recorded. The results are summarized in Figures 1–3 in the form of melting temperature (T_m)–crystallization temperature (T_c) plots. It is readily apparent that there are differences in behavior over this range of molecular weights.

The two lowest molecular weight fractions show very little change in melting temperature with the crystallization temperature. At most there is only a 1 °C increase in T_m for the 4–5 °C range in T_c. These results have a straightforward explanation if the samples form crystallites whose thicknesses are comparable to their extended-chain length over the entire isothermal range. This conclusion is supported by previous Raman LAM and small-angle

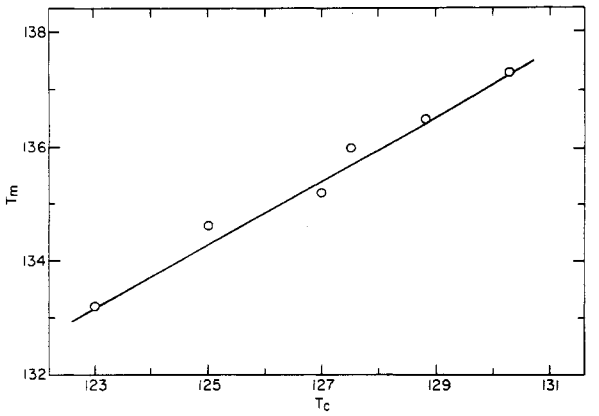

Figure 3. Plot of observed melting temperature, T_m, against crystallization temperature, T_c, for fraction M_w = 8400, M_n = 8000.

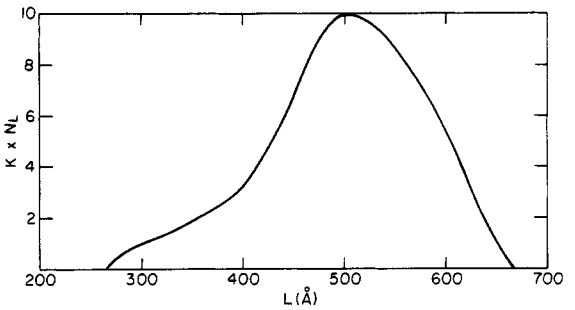

Figure 4. Plot of Raman-derived crystallite size distribution for fraction M_n = 5600 crystallized at 125 °C for 14 days.

X-ray scattering studies on narrowly distributed molecular weight samples in the range (1–3) × 10^3.[24-26] These experiments established that even upon quenching, extended-chain crystals are formed in this molecular weight range. It is therefore clear that all isothermal temperatures would yield this extended thickness, resulting in an invariant melting point. In the present context we define extended-chain crystals to mean that the crystallite thickness is *comparable* to the extended-chain length.[27]

The next two highest molecular weight samples, M_n = 3769 and M_n = 5600, show a unique and heretofore unreported behavior for polyethylene, as is illustrated in Figure 2. A significant increase in the melting temperature is observed with each of these polymers with only a small change in the crystallization temperature. For crystallization above and below this temperature, the melting temperatures are essentially invariant. A similar kind of crystallization temperature–melting temperature relation has been reported for poly(ethylene oxide) of molecular weight 3000–8000.[3] It has, however, not been observed previously in polyethylene. Above this jump temperature, the invariance in melting temperature is similar to what has been observed for the very low molecular weight samples described in Figure 1. These data thus suggest that extended-chain crystals are formed at the higher crystallization temperatures.

To verify the conclusion that extended-chain crystals are being formed under these conditions, the crystallite thickness distribution for M_n = 5600 after crystallization at 125 °C was calculated from its Raman-active longitudinal acoustic mode.[11-13] The crystallite size distribution is shown in Figure 4. It is centered at 500 Å, which is equivalent to its extended-chain length of 508 Å. The breadth of the distribution is consistent with the molecular weight distribution and the formation of extended-chain crystals. The crystallization behavior in the vicinity of the jump temperature will be analyzed in more detail shortly.

Table II[a]
Parameters Governing Fusion of Linear Polyethylene

M_n	x	T_m, °C	ζ_e	ζ_e/x	σ_e, cal/mol	$x - \zeta_e$
1586	113	124.5	95 ± 1	0.84 ± 0.01	1298 ± 200	18
2221	159	126.0	140 ± 2	0.88 ± 0.01	2024 ± 200	19
3769	269	132.0	242 ± 3	0.90 ± 0.01	2551 ± 300	27
5600	400	134.2	368 ± 4	0.92 ± 0.01	3485 ± 500	32

[a] Uncertainties calculated assuming $T_m = \pm 1$ °C.

For the highest molecular weight sample studied here, $M_n = 8000$, there is a continuous increase in the melting temperature with crystallization temperature. No discontinuity is observed in the melting temperature–crystallization temperature plot for this fraction. The Raman longitudinal mode indicates that a broad thickness distribution develops after long-time crystallization at 127 °C.[30] Even at this relatively low temperature the distribution contains crystallites having thicknesses that are comparable to the extended molecular length. This result is in agreement with early electron microscope studies of fracture surfaces, which reported that extended sizes could be formed up to molecular weights of 10 000 after crystallization for very long times at high temperatures.[28,29] The increase in melting point that occurs after crystallization at temperatures above 127 °C indicates that the endothermic peak must reflect some average of the very broad size distribution. Therefore, this peak melting point cannot be used as a measure of the melting of the extended-chain crystals that are known to be present. For the lower molecular weights, with a much narrower size distribution, the endothermic peak can be identified with the melting temperature of the extended-chain crystals.

There are essentially two main points in the experimental results summarized in Figures 1–4. One is the formation of extended-chain crystals and the other is the discontinuity in the T_m–T_c plots for specific low molecular weights. We shall consider, in turn, the implications of each of these results.

Theoretical Analysis. Having available the melting temperatures of extended-chain crystals presents us with the unique opportunity of examining the theoretical basis for the melting temperature–molecular weight relations. Similar data have been available for poly(ethylene oxide) fractions.[1,7] The analysis that was presented for these data was based on a modification of the Flory–Vrij equation.[1] A more detailed discussion of this work is given elsewhere[31] since the Flory–Vrij analysis requires the formation of molecular crystals where the ends are aligned and paired.[10,27] This condition cannot be met by any real system, no matter how well fractionated.[10,27] Hence, the equilibrium model is more properly taken as one where there is some element of disorder at the molecular ends.[27] The theoretical analysis given by Flory[32] is then most suitable for the real fractionated polymer system. Here the chain participates in only one crystallite and the end group is excluded from the lattice. The extended-chain crystals of low molecular weight that are being studied here clearly satisfy these criteria.

According to theory[32]

$$\frac{1}{T_{m,e}} - \frac{1}{T_m^\circ} = \frac{R}{\Delta H_u}\left(\frac{1}{x} + \frac{1}{x - \zeta_e + 1}\right) \quad (1)$$

$$2\sigma_e = RT_{m,e}\left\{\frac{\zeta_e}{x - \zeta_e + 1} + \ln\left(\frac{x - \zeta_e + 1}{x}\right)\right\} \quad (2)$$

Here, T_m° is the equilibrium melting temperature for an infinite molecular weight chain and $T_{m,e}$ is the corresponding temperature for a fraction containing x repeating units. σ_e can be considered to be the effective interfacial free energy associated with the basal plane of an equilibrium crystallite of length ζ_e, and ΔH_u is the enthalpy of fusion per repeating unit. Since we have shown that extended-chain crystals form in the low molecular weight range, the crystallites can obviously achieve equilibrium length. These melting temperatures can therefore be equated with $T_{m,e}$. It is difficult to obtain T_m° from eq 1 and 2 in terms of the attainable experimental data because the dependence of both σ_e and ζ_e on x needs to be known. On the other hand, if T_m° is known independently, then from the experimentally determined $T_{m,e}$ for a given x both σ_e and ζ_e can be obtained. This is the situation that exists for linear polyethylene. From analysis of the well-established data for the thermodynamics of fusion of the n-paraffins by means of the Flory–Vrij equation, T_m° was found to be 145.5 ± 1 °C for linear polyethylene.[10] Utilizing this value for T_m° and the measured melting temperature for each of the fractions that gave extended-chain crystals, we calculated the values of σ_e and ζ_e that are given in Table II. The ratio ζ_e/x increases with x and appears to be approaching a constant value. Concomitantly σ_e increases. This increase can be attributed to the first term on the right of eq 2, which reflects the number of ways the equilibrium length ζ_e can be selected from a chain of length x with chain ends excluded. This quantity would be expected to reach a constant value at somewhat higher molecular weights. The difference between x and ζ_e, given in the last column of Table II, increases with molecular weight. This trend would be expected to continue at the higher molecular weights.

The effective interfacial energy for crystallites forming extended-chain crystals, with significant disorder at the ends, is thus found to be of the order of 3000–4000 cal/mol of sequence. The interfacial free energy for mature, nonequilibrium crystallites, where the thickness is much smaller than extended length, is in the same range, i.e., about 4700 cal/mol.[29,33] Analysis of the crystallite size–crystallization temperature relation for solution-formed crystals by the most general aspects of nucleation theory yields similar values for the nucleation free energy.[33] Therefore, the assertion that regularly folded chains have a substantially lower interfacial free energy for nucleation, which is also characteristic of mature crystallites,[34] is not substantiated.

Melting temperature–molecular weight data are also available for poly(ethylene oxide) over the range M_n = 1100–7760 (x = 25–176) where extended-chain crystals are formed.[1] Values of T_m° can be obtained by extrapolating the dependence of the observed melting temperature on the crystallization temperature for high molecular weight fractions.[35,36] Utilizing this technique with poly(ethylene oxide), Beech and Booth[37] and Allen[38] reported values for T_m° of 76.0 and 80.0 °C. The analysis of the observed melting temperatures by means of eq 1 and 2 for extended-chain crystals yields similar values for σ_e and ζ_e/x, and their molecular weight dependence, as has been obtained with polyethylene. Booth[7] performed a similar analysis

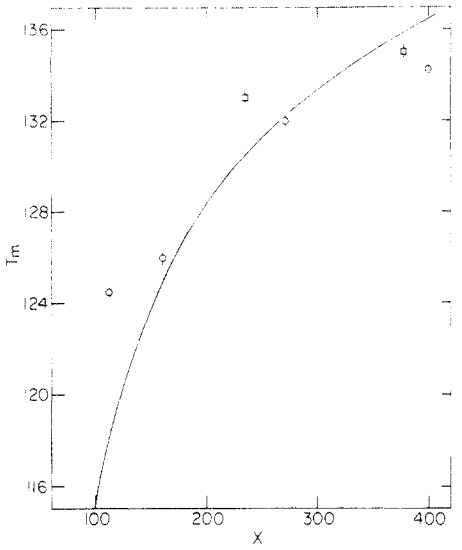

Figure 5. Plot of melting temperature against chain length x. Solid curve, n-paraffins from ref 10; (O) polyethylene fractions, this work; (□) from ref 27.

with poly(ethylene oxide) and found σ_e values of the same magnitude, which also increased with molecular weight.

The fact that σ_e and ζ_e/x are functions of chain length in the lower molecular weight range makes it impossible to describe the equilibrium melting relations as a simple function of chain length. Consequently, there is no obvious way that melting temperature data such as that obtained here can be used to perform an extrapolation to an unknown equilibrium melting temperature for an infinite chain.

In Figure 5 we have plotted the melting temperatures of the extended crystallites of the low molecular weight polyethylenes studied here against their number-average degree of polymerization. Results for two fractions previously reported[27] are also plotted. Previous studies which have compared the hydrocarbon melting temperatures with the polyethylene fractions have been restricted to a narrow molecular weight range with no sample below 3000.[27,39] Good agreement is found between these different studies where the data overlap. The curve drawn in this figure represents the melting temperature of the n-paraffins as a function of chain length. The data were obtained from the compilation and analysis given by Flory and Vrij.[10] At the lower molecular weights the melting temperatures of the polymers are greater than or comparable to those of the n-hydrocarbons. For the larger chain lengths the n-hydrocarbons are clearly more stable. The possibility of such behavior in the melting temperature–molecular weight data was indicated much earlier.[27] These results are a reflection of different effective interfacial free energies of each of the species and their molecular weight dependence. These results further emphasize the serious error that is involved in applying the Flory–Vrij analysis to molecular weight fractions, no matter how carefully the experiments are carried out.[1,8]

Crystallite Thickness. In addition to the observation of extended-chain crystals, the other major finding is the jump in the observed melting temperature for molecular weights in the range 3000–6000. One obvious explanation for the lower melting points is that thinner crystallites are formed at the lower crystallization temperatures. We consider this problem in more detail by focusing attention on the behavior of the M_n = 5600 sample. In Figure 6 the Raman-derived crystallite thickness distribution is given for this polymer when fully crystallized at 123 °C. This crystallization temperature is located below the jump in

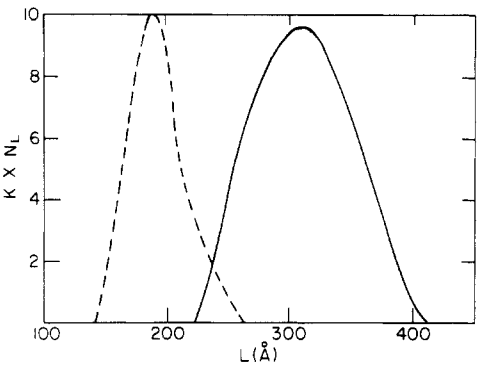

Figure 6. Plot of Raman-derived crystallite size distribution for fraction M_n = 5600: (—) crystallized at 123 °C for 28 days; (---) rapidly crystallized (quenched).

Table III[a,b]
Analysis of Melting Temperatures for Sample M_n = 5600

T_c, °C	ζ	ζ/x	T_m, °C	$\sigma_{e,c}$ cal/mol
quenched	146	0.36_5	129.5	2554 ± 400
123	244	0.61	132.7	3278 ± 500
125	394	0.98_5	134.2	3573 ± 500

[a] ζ given in CH_2 units. [b] Uncertainties calculated assuming T_m = ±1 °C and ζ = ±15.

melting point. From this distribution, which has a maximum at about 300 Å, it is clear that the crystallite sizes are very much smaller than those formed at the higher crystallization temperatures (see, for example, Figure 4). A quenched sample for M_n = 5600 was also studied. Its crystallite size distribution, also given in Figure 6, is relatively narrow. The maximum in the distribution for this crystallization mode is slightly less than 200 Å. Thus the peak value decreases from about 500 Å for crystallization at 125 °C to 200 Å for very rapid crystallization.

To see if the changes in the melting temperature are reasonable in terms of the differences in the crystallite thickness, the data were analyzed by eq 3, which describes

$$\frac{1}{T_m} - \frac{1}{T_m^\circ} = \frac{2\sigma_{e,c}}{\Delta H_u T_m \zeta} - \frac{R}{\Delta H_u \zeta} \ln\left(\frac{x - \zeta + 1}{x}\right) \quad (3)$$

the melting of crystallites of finite (nonequilibrium) size.[27] In this equation T_m is the melting point of a crystallite of thickness ζ, and $\sigma_{e,c}$ is the interfacial free energy associated with the mature nonequilibrium crystallite. By assuming that the observed melting temperature, as determined by differential calorimetry, corresponds to the peak size of the distribution, one can calculate the value of $\sigma_{e,c}$ for each sample. The results of these calculations are given in Table III. The values of $\sigma_{e,c}$ do not significantly differ among the three samples despite major differences in the relation of the crystallite thickness to extended-chain length. The two isothermally crystallized samples have about the same value within the experimental uncertainty; $\sigma_{e,c}$ for the quenched sample is just slightly lower.[48] The fact that the values of $\sigma_{e,c}$ for the two isothermally crystallized samples are virtually identical indicates that the difference in melting temperature must be explained by the thickness differences. It does not reflect any differences in the surface structure as would be reflected in the interfacial free energy. The problem that remains to be resolved, therefore, is why a very small increase in the crystallization temperature, only about 1 °C, causes such a large change in thickness.

To address this question in more detail the crystallization process at each of these isothermal temperatures was

Table IV
Thermodynamic Data during Course of Isothermal Crystallization for M_n = 5600

time, min	T_m, °C	$1-\lambda^a$	$1-\lambda^b$
	(a) At 125 °C		
75	132.8	15	74
87.5	133.1	19	78
100	133.7	38	82
110	133.7	48	86
120	133.6	57	88
225	134.4	69	90
450	133.9	76	94
1700	133.9	83	94
20000	134.2	83	94
60000	134.6	84	95
	(b) At 123 °C		
5.5	130	(8.5)	78.5
7	129.6	(21)	78.5
8.5	130.3	47	79
10.5	131.7	70	84
15	132.0	72	83
30	133.1	77	88
100	133.0	79	87
80000	132.7	87	94

[a] Degree of crystallinity, from enthalpy of fusion, at isothermal crystallization temperature. [b] Degree of crystallinity, from enthalpy of fusion, at room temperature.

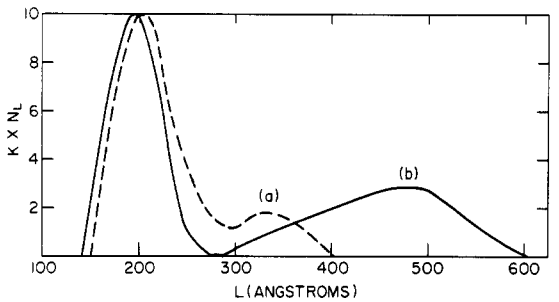

Figure 7. Plot of Raman-derived crystallite size distribution for fraction M_n = 5600 crystallized at 125 °C: (a) after 75 min; (b) after 120 min.

studied by examining samples that had been crystallized for different times at the respective temperatures. The thermodynamic data for the samples crystallized at 125 °C are listed in Table IVa. For those samples that were not fully crystallized at the isothermal temperature, two melting peaks are observed in the differential calorimeter. One is due to crystallites formed at the isothermal temperature, and the other is due to those formed upon cooling. The amount of crystallinity formed at the isothermal temperature can thus be calculated from the heat of fusion assigned to the higher melting peak. Although there is some uncertainty in this method because of a slight overlap of the two peaks, it is adequate for establishing in what stage of the crystallization process a given sample was removed for study. This is all that is necessary for present purposes.

Figure 7 gives the crystallite thickness distribution, as determined from the Raman analysis, for two early crystallization times at 125 °C. In these two distributions the peak centered around 200 Å is due to crystals formed during the cooling process; the smaller peak at higher spacings is due to those crystals formed at the isothermal temperature. The distribution for the sample crystallized for 75 min, corresponding to 15% isothermal crystallization, shows that the thicknesses of initial crystallites that form at this temperature are not comparable to the extended-chain length. In the sample crystallized for 120

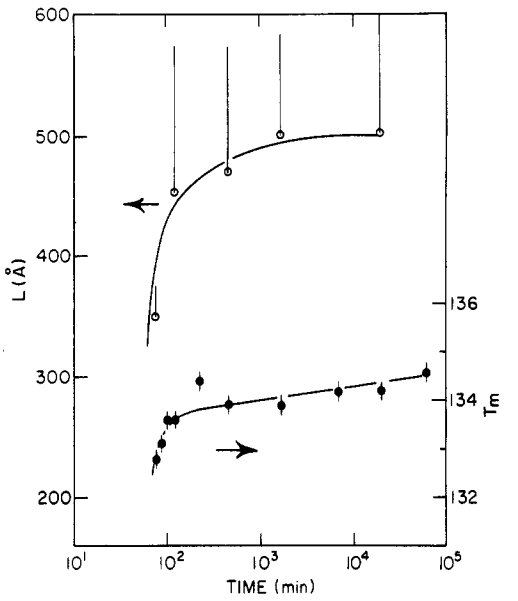

Figure 8. Plot of crystallite thickness (half-width at half-height) and melting temperature as a function of log time at 125 °C for M_n = 5600: (○) crystallite thickness; (●) melting temperature.

min, where the isothermal crystallinity is now 57%, the size distribution has increased substantially and is approaching the distribution present in the sample crystallized for long times (see Figure 4). It is thus apparent that at this temperature and for this molecular weight, small crystallites that are initially formed rapid grow to extended length in the very early stages of the crystallization process.

To describe graphically the process in a more convenient way, each distribution is represented by a vertical line. The lowest point (solid circle) corresponds to the most probable thickness. The line is drawn upward from this point and the terminus represents the largest crystallite size at half-height.[40] The lower half of the distribution is not represented because of overlap with the quenched sizes. By adopting this procedure, we represent in Figure 8 the change in crystallite thickness as a function of the logarithm of time. This figure demonstrates even more vividly the conclusions drawn above. The initial small thickness distribution increases rapidly to essentially extended-chain thickness and then there is only a slight increase with crystallization over many decades of time. The corresponding peak melting temperatures are also plotted in this figure. The melting point data are consistent with the thickness observations. The melting temperature increases rapidly during the early stages of crystallization, where significant thickening occurs. At much longer times the melting temperature remains invariant, reflecting the thickness distribution being centered around the extended-chain length and thus remaining constant.

A similar study was carried out for the crystallization at 123 °C. The thermodynamic data for each of the crystallization times sampled are given in Table IVb. At the very early times there is no detectable isothermal melting peak in the calorimeter traces. However, from the measured isothermal crystallinity developed at later times, it is possible, by use of the Avrami equation,[41,42] to approximate the amount of isothermal crystallinity that must have been present at the early stages. The fact that this crystallinity is not detected suggests that melting occurs at a low enough temperature to be obscured by the melting of the quenched material. The shortest time of crystallization for which a separate peak, corresponding to the isothermally formed crystallites, can be observed in the

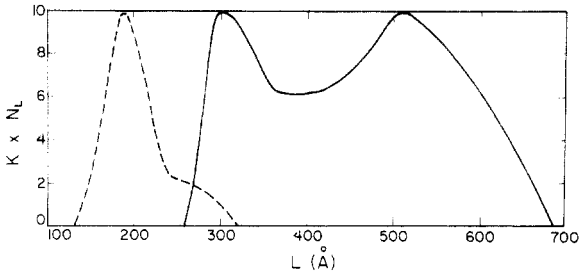

Figure 9. Plot of Raman-derived crystallite size distribution for fraction M_n = 5600: (---) crystallized at 123 °C for 7 min; (—) crystallized at 124 °C for 10 days.

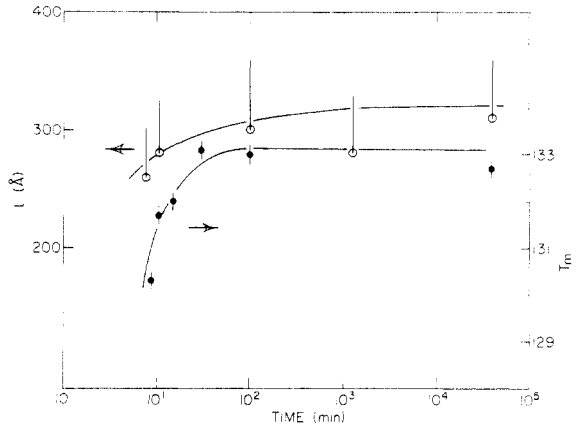

Figure 10. Plot of crystallite thickness (half-width at half-height) and melting temperature as a function of log time at 123 °C for M_n = 5600: (○) crystallite thickness; (●) melting temperature.

Raman LAM occurs at 7 min. The crystallite size distribution for this sample, plotted in Figure 9, clearly has a distinct peak at higher spacings. However, this peak corresponds to a smaller crystallite thickness than is found in the 125 °C sample having comparable isothermal crystallinity. Comparison of the 7-min distribution to that obtained after crystallization for very long times at 123 °C (see Figure 6) shows that only a slight increase in the crystallite sizes has occurred with time.

This conclusion is demonstrated more clearly in Figure 10, where the distributions for each crystallization time are plotted as a function of log time. This plot indicates a very slight increase in the size distribution at the very early times. However, the major conclusion is clearly that there is no change in the size distribution during the last two decades of time that the sample is kept at the isothermal temperature. The melting temperatures are also plotted in Figure 10. At the longer crystallization times the melting temperatures are invariant and are thus consistent with the constancy in crystallite thickness. At the lower times there is an apparent increase in melting temperature. However, as has been indicated, the isothermal peak is not resolved here. In this situation, therefore, the peak melting temperature might not represent the isothermally crystallized sizes.

A sample crystallized at 124 °C for a long time, i.e., between the two extreme crystallization temperatures, has a melting point corresponding to the 125 °C crystallization. The Raman-derived distribution for this temperature, after crystallization for 10 days, is also given in Figure 9. Crystallites having thicknesses comparable to those formed at 125 °C are present in appreciable concentration and their presence explains the high melting point. However, the size distribution is much broader than the 125 °C crystallized sample, with a significant concentration of smaller sizes being present. The distribution at 124 °C indicates that not all the crystallites in the sample are able to grow to extended-chain length, even after long-time crystallization.

The size analyses given above show that the sudden increase in crystallite thickness, and in the melting temperature, for just a small change in crystallization can be explained by the fact that the crystallites formed at 125 °C grow to extended length at that temperature. In contrast, those crystallites initially formed at 123 °C do not substantially change their size. Higher molecular weight fractions give quite different results. Here, although the thickening process is very temperature dependent, increases in crystallite size occur during the complete course of crystallization and at all isothermal temperatures.[30,40,43] No discontinuities are found with crystallization temperature. The size increases gradually, as opposed to the rapid growth that is observed with the low molecular weight samples.

The two likely causes for the discontinuity observed at the lower molecular weights are (i) that crystallites formed at the two temperatures have some type of structural difference and (ii) that in fact, they are similar but storage at 125 °C allows for growth while 123 °C is too low a temperature. To help decide between these possibilities a sample was first crystallized at 123 °C and then transferred to 125 °C. After storage for 1 month at 125 °C the sample was found to give the same melting point as if crystallized and maintained at 123 °C. This result strongly suggests that the discontinuity in melting temperatures is caused by differences in the crystallites initially formed at the two temperatures. The crystallite size distribution observed for early crystallization times at the two temperatures is consistent with this conclusion since differences are observed in the crystallites formed isothermally.

To investigate this possibility we examine possible differences in nuclei sizes formed at these two temperatures. The sizes observed at early crystallization times cannot be equated to nuclei sizes because some thickening of the nuclei may have already occurred. However, they can serve as upper limits. Thus, calculations using nucleation theory of finite chains were made[44] to see if significant differences are predicted between nuclei sizes at 123 and 125 °C. Nucleation theory defines the minimum thickness needed to have a stable nucleus ζ^* at a given temperature. For chains of finite molecular weight[44]

$$\frac{\zeta^*}{2}\left[\Delta f_u - \frac{RT}{x} + \frac{RT}{x - \zeta^* + 1}\right] = 2\sigma_{en} - RT \ln\left(\frac{x - \zeta^* + 1}{x}\right) \quad (4)$$

Here, σ_{en} is the interfacial free energy for nucleation and Δf_u is the free energy of fusion per repeating unit. It should be noted that σ_{en} is not the same as σ_e or σ_{ec}, the interfacial free energies that have been previously introduced.[36] Equation 4 does not allow for an absolute determination of ζ^* unless σ_{en} is known. Thus, ζ^* was calculated as a function of temperature for M_n = 5600, assuming different values for σ_{en}. In this way a family of curves was generated; the results are plotted in Figure 11. In the temperature interval of interest, between 123 and 125 °C, ζ^* increases by about 20 units for the interfacial free energy values considered. These values for the interfacial free energy are reasonable and consistent with those deduced for the mature crystallites. The values for ζ^* that are calculated are of the order of 0.5–0.6 that of the extended-chain length. The results of this admittedly approximate calculation suggest a possible explanation for the discontin-

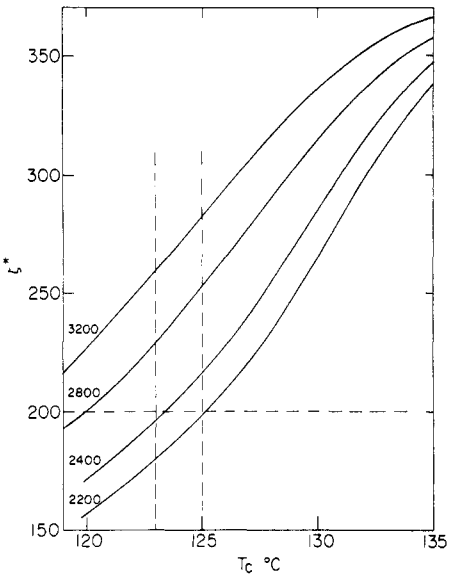

Figure 11. Calculated critical nucleus size, ζ^* (in CH_2 units), plotted against crystallization temperature, T_c, for different values of interfacial free energy. Calculations carried out according to eq 4.

uities in crystallite thicknesses, which are then reflected in the respective melting temperatures.

After formation of the initial nucleus the remaining free chain units of each molecule are, in principle, capable of crystallizing by *c*-axis growth to extended-chain crystallites. This process would be retarded if the sequences were sufficiently long so that they could crystallize within the already formed lamellae. The previous calculations indicate that the size of the nucleus increases significantly between 123 and 125 °C and is approximately half the chain's extended length at the higher temperature. This increase in size could have the effect of making the remainder of the chain too short to crystallize, while maintaining the lamella thickness. Even if the initially noncrystalline sequences were large enough to crystallize, it is possible that *c*-axis growth would still occur. There must be a competition between *c*-axis growth, lamellar growth, and even the formation of new crystallites. The latter two processes are nucleation controlled and hence very sensitive to the crystallization temperature. They would be retarded at the higher crystallization temperature, while *c*-axis growth would not since it is not nucleation controlled. Hence *c*-axis growth would not change significantly between 123 and 125 °C. The net effect would be that at 125 °C there would be a much greater chance of *c*-axis growth as contrasted with processes involving an additional nucleation act. It is difficult to decide whether differences in the initial nuclei sizes or in the rates of nucleation in the growth processes explain the observed jump in thickness. Both factors operate in the same direction and their combined effects cause the abrupt changes that are observed. These considerations would not, of course, apply to higher molecular weight fractions, where major increases in crystallite size distribution are observed by a quite different mechanism.[30,40,43] As the melting point data of Figures 1–3 indicate, it takes unique molecular weights and crystallization temperatures to observe these effects. This is consistent with the nucleation origin of this phenomenon where the effect would be restricted to low molecular weights.

A comparison of the peak sizes, as well as the complete crystallite thickness distributions, after long-time crystallization at 123 and 125 °C, shown in Figures 4 and 6, makes very clear that the sizes in the two cases do not differ by a factor of 2. Such an exact integral relation in the crystallite thicknesses has been deduced for low molecular weight poly(ethylene oxide).[2] This conclusion was based on small-angle X-ray scattering studies which yielded average thicknesses but not the entire thickness distribution.[2] It is therefore impossible to say whether the actual distribution present had a breadth comparable to that in the present case for polyethylene. It is, however, possible to compare some of the other experimental observations for low molecular weight poly(ethylene oxide) with those found here. Multiple melting peaks were commonly seen in poly(ethylene oxide), with more of the higher melting peak present at higher crystallization temperatures.[3] Although multiple melting was not observed in the present work, the broad distribution present after crystallization at 124 °C suggests a similar situation. Here appreciable concentrations of crystallites corresponding to both melting points are present. However, only the higher melting peak is resolvable in the DSC trace.

In a light microscope study, Kovacs[4] was able to distinguish the regions of poly(ethylene oxide) crystals that have reached extended length. He was thus able to study the thickening process and determined that growth to extended-chain length occurs during the early stages of the crystallization process. This is analogous to the Raman measurements for the polyethylene crystallized at 125 °C, which show that growth to extended size occurs very rapidly. These similarities in the two polymers suggest that the jumps seen in poly(ethylene oxide) may have the same basic explanation.

Morphology and Structure. The unique size relations, relative to the molecular length, that are found in these low molecular weight fractions make it of interest to study their crystallite structure. The character of the crystallites for molecular weight fractions from $M = 2.78 \times 10^4$ to 6.0×10^6 has been studied previously by means of thin-section transmission electron microscopy.[15] We found that there was a continuous change in the nature of the crystallite with increasing molecular weight. The large lamellar platelets observed at the lower molecular weights become shorter roof-shaped lamellae at intermediate molecular weights and eventually yield curved crystals at the highest molecular weights.[15] A similar tendency was found as the undercooling at which the crystallization was conducted was increased.[15,16] Qualitatively similar results have been reported by Bassett and Hodge,[45] without, however, a detailed quantitative analysis. Studying the molecular weight fraction $M_n = 5600$ is then of interest, particularly in view of its thermodynamic and kinetic properties.

Transmission electron micrographs for $M_n = 5600$ crystallized at three different temperatures are given in Figures 12–15. For the low molecular weight sample under discussion here we find that even the quenching procedure gives roof-shaped lamellae with a lateral extension of several microns (Figure 12). This situation had only been previously observed for intermediate molecular weights isothermally crystallized at high temperature.[15] As can be seen in Figure 12, the lamellae frequently form "roofs" in a cooperative manner. This is indicated by positions A, B, and C in the micrograph. However, many regions have a "disorganized" appearance, such as the one marked D.

Figure 13 gives the results for the same sample crystallized at 123 °C. The general impression is created that the lateral extension of the lamellae has increased. A more drastic change is indicated in Figure 14 for the specimen that was crystallized at 125 °C. Here, there is clearly a dramatic increase in the crystal thickness, while at the

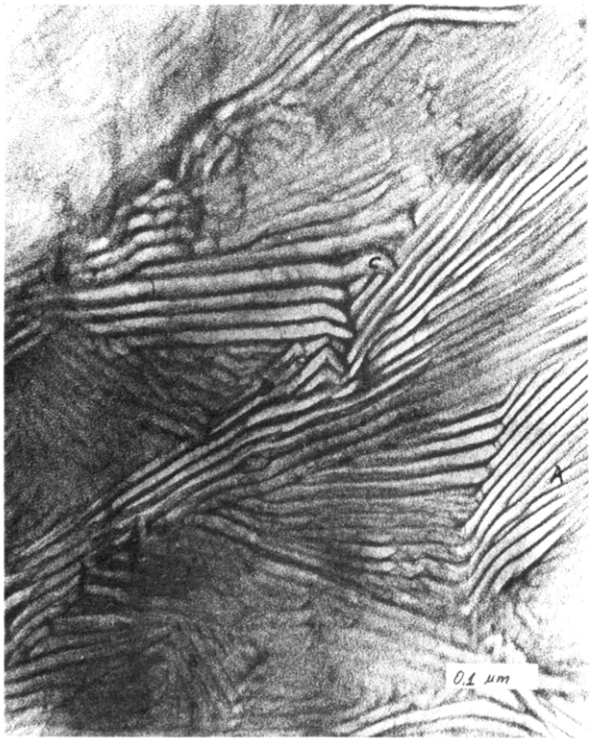

Figure 12. Transmission electron micrograph of fraction M_n = 5.6×10^3 (quenched).

Figure 13. Transmission electron micrograph of fraction M_n = 5.6×10^3 crystallized at 123 °C.

same time the thickness distribution has become very broad. The thickest crystal in the center of the micrograph consists of extended-chain molecules. The thinnest lamellae are only about 100 Å thick and were formed during the cooling process subsequent to the isothermal crystallization. They are not really pertinent to the crystallization at 125 °C. Other crystals have intermediate thicknesses. While this polydisperse size situation is common, homogeneous areas are also observed. An example is given in Figure 15. The total distance over which the crystalline lamellae extend in a cooperative manner in the chain direction is well beyond the extended-chain length. In the

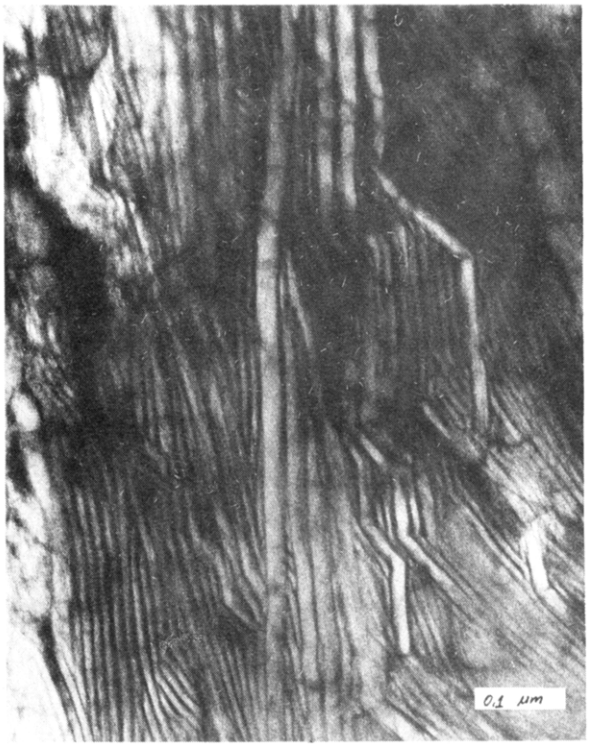

Figure 14. Transmission electron micrograph of fraction M_n = 5.6×10^3 crystallized at 125 °C.

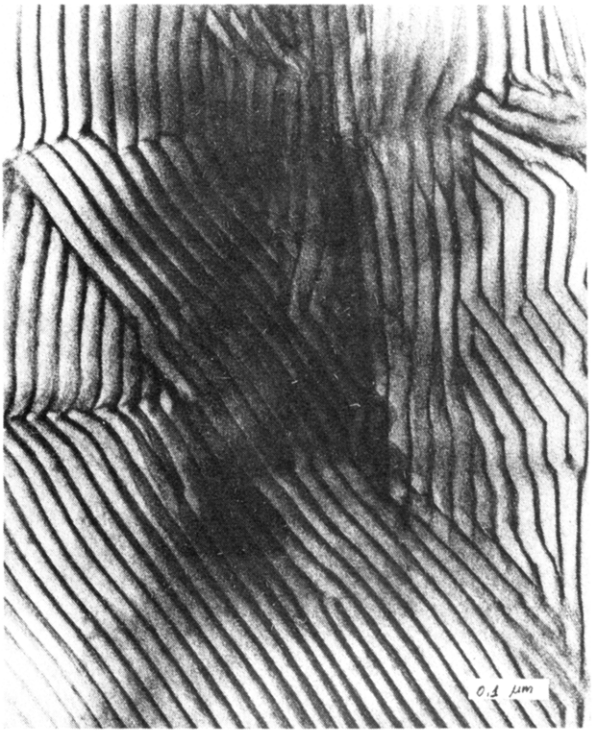

Figure 15. Detailed transmission electron micrograph of fraction $M_n = 5.6 \times 10^3$ crystallized at 125 °C.

course of our work we have also studied a very low molecular weight fraction (M_w = 1000) which consists entirely of extended-chain crystals.[25,26] It was impossible to obtain contrast at any time with this sample. Clearly, the staining medium cannot penetrate the surface layers in this situation. Consequently the stained regions for the M_w = 5600 samples would not be expected to represent the extended-chain crystals. Such crystals are known to be present from the Raman measurements. Rather, a select view will be obtained of those regions not containing such crystals.

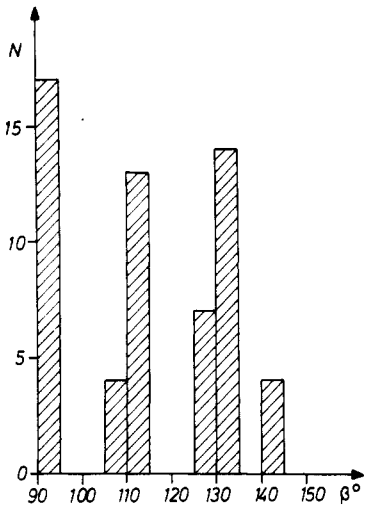

Figure 16. Analysis of observed apex angle β for the quenched sample.

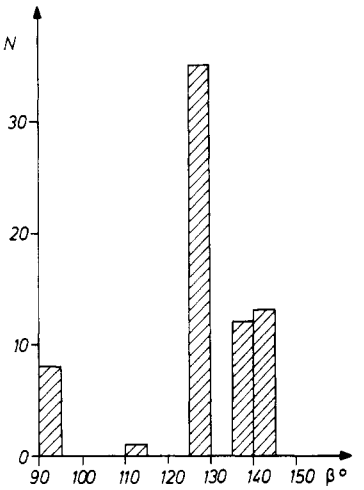

Figure 17. Analysis of observed apex angle β for sample crystallized at 123 °C, M_n = 5600.

There is only one exception to this rule, namely, whenever a single extended-chain lamellae is surrounded by thinner crystallites with disordered interfacial layers.

The "roof" apex angles are well-defined for all the specimens of this molecular weight that were studied. They can be determined by crystallographic methods which have been described in detail.[15] Figures 16–18 are histograms of the measured apex angles for the quenched sample and the samples crystallized at 123 and 125 °C, respectively. The quenched sample (Figure 16) shows six main angular regions, located at about 90, 107, 112, 126, 135, and 144°. The percentage of crystallites having the 90, 107, and 112° apex angle is large for this sample. The proportion of these smaller angles decreases for crystallization at 123 °C and finally disappears at the higher crystallization temperature. At the same time, with increasing crystallization temperature there is an increase in the proportion of crystals with the larger apex angles. For example, from Figure 18, representing crystallization at 125 °C, it is clear that the apex angle of 144° predominates. Since the apex angles reflect the internal structure of the crystallites, a closer scrutiny of these results is in order. The internal structure of the crystallites is changing with the crystallization conditions.

We have shown previously[15] that the apex angles 90, 112, 126, and 144° are the angles between the {301}, {201}, {302}, and {101} planes. The apex angles of about 107 and 135° do not fit into this category of single planes and they must

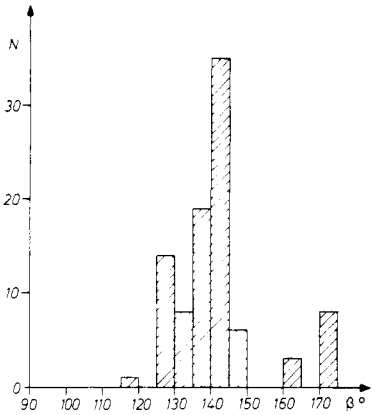

Figure 18. Analysis of observed apex angle β for sample crystallized at 125 °C, M_n = 5600.

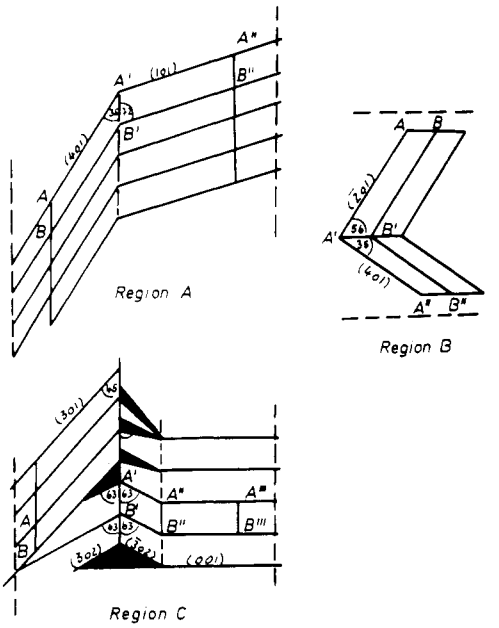

Figure 19. Analysis of regions A, B, and C from the electron micrograph of Figure 12.

represent a combination of different planes. We analyze this situation in the following way. The drawing of Figure 19 was obtained by transferring the most relevant details from Figure 12 onto transparent paper. On this drawing the tips of the apex angles in each stack are connected by a dotted line which thus indicates the molecular chain direction. The analysis of region A immediately shows the origin of the apex angle of 107°. It results from a combination of the {401} and {101} planes. The possible combinations of many other planes are indicated in Figure 2 to aid in the discussion.

Similar analysis shows that the angle of about 90° in region B is not the included angle between the {301} planes, each inclined at 45° to the molecular axis. Rather it is the angle between the {201} and {401} planes, inclined at 35 and 56° to the molecular axes, respectively. In both of these cases a drastic change in lamellar thickness occurs where the two planes meet along the roof gable. This change in thickness is easily accounted for in Figure 19. The molecular chain direction is determined by the line connecting the apex angles. Consequently the stem length stays identical within one lamella; i.e., AB = A′B′ = A″B″. Measurement along the chain direction indicates that AB corresponds to a chain length of about 180 Å. At this molecular weight, the extended-chain length is approximately 500 Å, corresponding to the molecular length

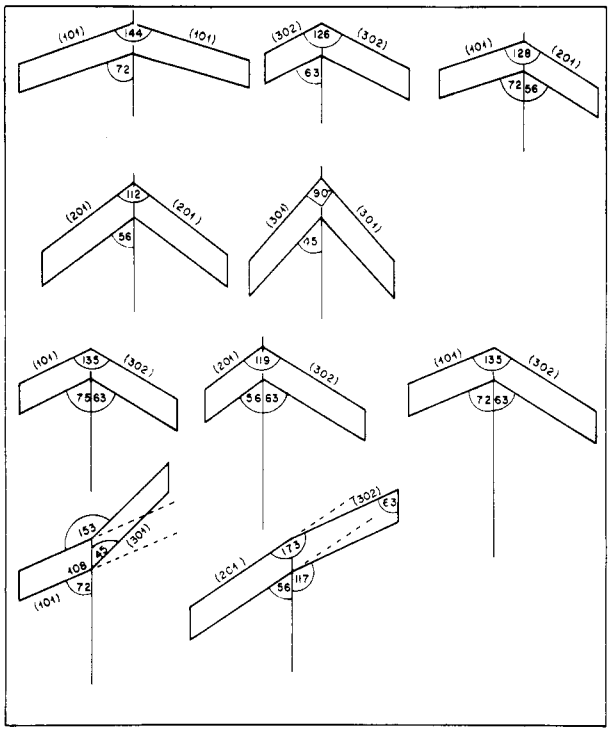

Figure 20. Relationship between intersecting crystallographic planes and apex angles.

through a stack of 2–3 lamellae.

Region C is somewhat more complicated to analyze. Interlamellar contrast variations are observed, which appear at first sight to be somewhat confusing. However, the drawing in Figure 19 indicates that, in each case, the gray, interlamellar contrast arises when the lamellar surface planes are changing, in this case from {301} to {302}. Hence there is a mismatch at the "roof" tip. This mismatch causes such an extent of molecular disorientation that the staining medium can penetrate.

The detailed analysis of the apex angles observed at 125 °C crystallization indicates the absence of the very small values in the vicinity of 90–110°. This result suggests that the very high chain tilt angles are less frequent for this crystallization condition. Here the apex angles that correspond to 36 and 18° tilts predominate. Figure 14 shows that the correct choice of a representative area corresponding to the actual crystallization temperature is very difficult. Nevertheless, an analysis of another region of this specimen, shown in Figure 15, has yielded some very important new aspects. This region shows a well-ordered lamellar geometry extending well beyond the molecular length. By joining apex angles as described previously, we observe that molecular orientation is retained over large regions. It extends over several thousand angstroms in the chain direction. Analysis of the apex angles from Figure 15 as is given in Figure 21 indicates a predominance of the {101}, {302}, and {201} surface planes, with a corresponding increased tendency toward the smaller tilt angles. This conclusion is also reflected in the analysis of the apex angles shown in Figure 18.

There is the very strong suggestion here that the molecular tilt angle is dependent on the crystallization temperature. Similar results are found with higher molecular weight samples and will be discussed in detail in a forthcoming paper.[17] This result can have far-reaching implications to crystallization kinetics and interfacial structure.

The micrograph shows quite clearly that, even within a single lamella, the tile angle with respect to the surface normal can change while the molecules retain their mutual

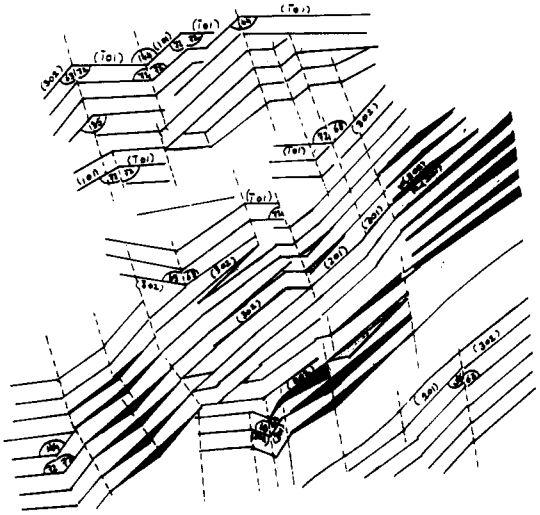

Figure 21. Relationship between morphology and molecular tilt within an area comprising about one square micron for sample crystallized at 125 °C (M_n = 5600).

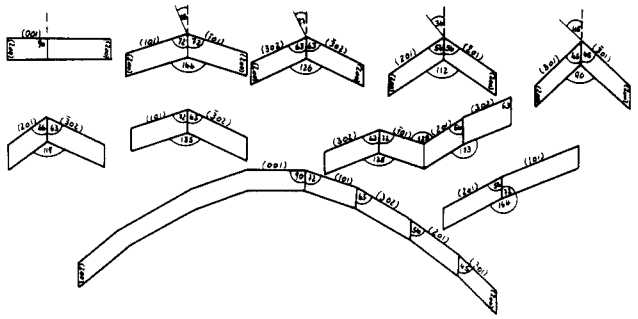

Figure 22. Molecular tilts calculated from observed apex angles for sample crystallized at 125 °C showing transition from "roof-shaped" to curved morphology.

orientation within the sample. That is, the external geometry may change while the direction of the molecule is undisturbed. Nevertheless, the lamellae surface planes are always well-defined crystallographic planes. Furthermore, in those cases where "roofs" are observed, i.e., where contrast is such that both planes on either side of the roof tip are simultaneously oriented parallel to the viewing direction, the crystallographic b direction is generally perpendicular to the plane of the paper. The fact that all the observed planes can be given indices of the $\{h0l\}$ type supports this view. However, such micrographs always represent a very select view, and other apex angles may occur that do not satisfy the conditions for contrast or do so less frequently.

Curved lamellae are now well-established crystallite forms which are most predominant for higher molecular weights and crystallization at large undercoolings.[15,16] The curvature of the crystallites can be explained by a change of the molecular tile with respect to the lamellar surface. In Figure 22 we illustrate how this curvature can evolve utilizing the sets of apex angles found for the low molecular weight samples studied here. The transition from a planar to roof-shaped to curved crystallite is thus brought about by the appropriate change in the molecular tilt angle.

The results of the electron microscopy study of specimen M_n = 5600 are consistent with earlier work.[15,16] With decreasing molecular weight, for the same crystallization temperature, lamellae develop from curved, via roof or multiple roof-shaped structures, to large, flat sheets. An increase in crystallization temperature increases the molecular weight at which a well-formed geometric morphology can be achieved. For the low molecular weight

samples, curvature is eliminated since apparently a sufficiently low crystallization temperature cannot be achieved. The micrographs in Figures 12–15 show that the roof-shaped structures are well defined. There is a tendency for sheetlike structures to develop at the higher crystallization temperatures.

We have also observed some unusual "roof angles" with these specimens. The angles of 112, 126, and 144° are easily accounted for by intersecting {201}, {302}, and {101} planes. However, the other angles involved cannot be accounted for by the intersection of these planes. Since it is well established that the roof gables lie along the crystallographic *b* axis,[16,45] it would be unreasonable to look for intersecting {*hkl*} planes in order to explain these angles. The micrographs themselves give the clue as to the origin of these angles. In some cases the crystal thickness is different on either of the two roof sides. When several roof-shaped crystals are packed within one another, it is found that the two angles on each side of a line joining their apices are not always identical. These angles correspond very closely, however, to the intersection between the $\{h_1 0 l_1\}$ and $\{h_2 0 l_2\}$ planes. The planes in question are {101}, {302}, {201}, and {401} in various combinations. This analysis means that there are different surface planes along a single lamella; i.e., different molecular tilts may arise along one lamella. Consequently, the available space and molecular orientation are determining factors as to which surface plane is formed during crystallization. These factors are in turn a function of molecular weight and crystallization temperature.

There is a definite tendency for the lower indexed surface planes to be developed at higher crystallization temperatures. This in turn means that the molecular tilt becomes smaller. Consequently, the available surface area per molecule emerging from the crystal surface decreases. This would require that the intermediate layers between the crystaline and amorphous regions be increasingly more ordered. Conversely, at the lower crystallization temperatures, with the larger tilt angles, the spatial problem is severely reduced as is then the restriction on the chain flux emanating from the basal plane.[46]

Acknowledgment. We are indebted to Mr. G. Weber, who carefully performed much of the preparation work. Support of this work by NATO Research Grant No. 1421, the Deutsch Forschungsgemeinschaft (Sonderforschungsbereich 41), and Exxon Chemical Corp. is gratefully acknowledged.

Registry No. Polyethylene (homopolymer), 9002-88-4.

References and Notes

(1) Buckley, C. P.; Kovacs, A. J. *Prog. Colloid Polym. Sci.* **1975**, *58*, 44.
(2) Spegt, P. *Makromol. Chem.* **1970**, *140*, 167.
(3) Buckley, C. P.; Kovacs, A. J. *Colloid Polym. Sci.* **1976**, *254*, 695.
(4) Kovacs, A. J.; Straupe, C. *Discuss. Faraday Soc.* **1979**, *68*, 225.
(5) Marco, C.; Fatou, J. G.; Bello, A.; Blanco, A. *Polymer* **1979**, *20*, 1250.
(6) Hay, J. N. *J. Polym. Sci., Polym. Chem. Ed.* **1976**, *14*, 2845.
(7) Beech, D. R.; Booth, C.; Pickles, C. J.; Sharpe, R. R.; Waring, J. R. S. *Polymer* **1972**, *13*, 246.
(8) Wunderlich, B.; Czornyj, G. *Macromolecules* **1977**, *10*, 960.
(9) Broadhurst, M. G. *J. Chem. Phys.* **1962**, *36*, 2578.
(10) Flory, P. J.; Vrij, A. *J. Am. Chem. Soc.* **1963**, *85*, 3548.
(11) Snyder, R. G.; Krause, S. J.; Scherer, J. R. *J. Polym. Sci., Polym. Phys. Ed.* **1978**, *16*, 1593.
(12) Snyder, R. G.; Scherer, J. R. *J. Polym. Sci., Polym. Phys. Ed.* **1980**, *18*, 1421.
(13) Glotin, M.; Mandelkern, L. *J. Polym. Sci., Polym. Phys. Ed.* **1983**, *21*, 29.
(14) Kanig, G. *Prog. Colloid Polym. Sci.* **1975**, *57*, 176.
(15) Voigt-Martin, I. G.; Fischer, E. W.; Mandelkern, L. *J. Polym. Sci., Polym. Phys. Ed.* **1980**, *18*, 2347.
(16) Voigt-Martin, I. G.; Mandelkern, L. *J. Polym. Sci., Polym. Phys. Ed.* **1981**, *19*, 1769.
(17) Voigt-Martin, I. G.; Mandelkern, L., submitted for publication.
(18) Go, S.; Kloos, F.; Mandelkern, L., in preparation.
(19) Kloos, F.; Go, S.; Mandelkern, L. *J. Polym. Sci., Polym. Phys. Ed.* **1974**, *12*, 1145.
(20) Popli, R.; Glotin, M.; Mandelkern, L.; Benson, R. S. *J. Polym. Sci., Polym. Phys. Ed.*, in press.
(21) Mandelkern, L.; Fatou, J. G.; Denison, R.; Justin, J. *J. Polym. Sci.* **1965**, *3*, 803.
(22) Harrison, I. R.; Varnell, W. D. *J. Thermal Anal.*, in press.
(23) Mandelkern, L.; Stack, G. M.; Mathieu, P. J. M. *Anal. Calorimetry*, in press.
(24) Glotin, M.; Mandelkern, L. *J. Polym. Sci., Polym. Lett. Ed.* **1983**, *21*, 807.
(25) Smith, P.; St. John Manley, R. *Macromolecules* **1979**, *12*, 483.
(26) Shu, P. H. C.; Burchell, D. J.; Hsu, S. L. *J. Polym. Sci., Polym. Phys. Ed.* **1980**, *18*, 1421.
(27) Fatou, J. G.; Mandelkern, L. *J. Phys. Chem.* **1965**, *69*, 417.
(28) Anderson, F. R. *J. Appl. Phys.* **1964**, *35*, 64.
(29) Mandelkern, L.; Price, J. M.; Gopalan, M.; Fatou, J. G. *J. Polym. Sci., Part A-2* **1966**, *4*, 385.
(30) Stack, G. M. Ph. D. Dissertation, Florida State University, Aug 1983.
(31) Mandelkern, L.; Stack, G. M. *Macromolecules*, in press.
(32) Flory, P. J. *J. Chem. Phys.* **1949**, *17*, 223.
(33) Mandelkern, L. *Polym. Eng. Sci.* **1969**, *9*, 255.
(34) Lauritzen, J. I.; Hoffman, J. D. *J. Res. Natl. Bur. Stand. Sect. A* **1960**, *64*, 73.
(35) Hoffman, J. D.; Weeks, J. J. *J. Res. Natl. Bur. Stand., Sect. A* **1962**, *66*, 13.
(36) Gopalan, M. R.; Mandelkern, L. *J. Phys. Chem.* **1967**, *71*, 3833.
(37) Beech, D. R.; Booth, C. *J. Polym. Sci., Part B* **1970**, *8*, 731.
(38) Allen, R. C. M. S. Thesis, Florida State University, Dec 1980.
(39) Takamizawa, K.; Oyama, T., private communication.
(40) Stack, G. M.; Mandelkern, L.; Voigt-Martin, I. G. *Polym. Bull.* **1982**, *8*, 421.
(41) Avrami, M. *J. Chem. Phys.* **1939**, *7*, 1103.
(42) Mandelkern, L. "Crystallization of Polymers"; McGraw-Hill: New York, 1964.
(43) Chivers, R. A.; Barham, P. J.; Martinez-Salazar, J.; Keller, A. *J. Polym. Sci., Polym. Phys. Ed.* **1982**, *20*, 1717.
(44) Fatou, J. G.; Howard, C.; Mandelkern, L. *J. Phys. Chem.* **1964**, *68*, 3386.
(45) Bassett, D. C.; Hodge, A. M. *Proc. R. Soc. London, Ser. A* **1981**, *377*, 25.
(46) Flory, P. J. *J. Am. Chem. Soc.* **1962**, *84*, 2857.
(47) This Raman method gives the distribution of ordered sequence lengths. In order to compare these results with lamellar thicknesses the inclination of the chain axis needs to be specified.
(48) We note the general possibility that the interfacial free energy of the mature crystallites might vary with crystallite thickness and crystallization temperature, if there is an accompanying change in the interfacial structure.